PAPER

Orientational order in a glass of charged platelets with a concentration gradient

Elisabeth Lindbo Hansen,[*a] Sara Jabbari-Farouji,[b] Henrik Mauroy,[c] Tomás S. Plivelic,[d] Daniel Bonn[e] and Jon Otto Fossum[a]

Colloidal dispersions of anisometric particles can display dynamical arrest and ordering involving both translational and rotational degrees of freedom. We show that orientational order can develop in glassy colloidal dispersions of charged platelets when a concentration gradient is imposed through solvent evaporation. Our model system of Laponite (LRD) platelets in deionized water has been extensively studied for its ergodic to non-ergodic transitions, and the existence of an underlying isotropic–nematic phase transition has been a subject of debate. We use small-angle X-ray scattering, dynamical light scattering and birefringence to show that the orientational order we observe does not result from an underlying, uniquely determined equilibrium state with orientational order, but from plastic deformation of the colloidal glass.

1 Introduction

Soft solids formed from colloidal dispersions are intriguing states of matter whose solid-like nature is attributed either to the formation of percolating networks (in gels) or to emerging topological constraints and dynamical correlations from crowding (in glasses). In this context, soft solids formed from anisometric particles such as clays are interesting because they can display arrest and ordering not only of translational but also rotational degrees of freedom. Experiments, simulations, and theory in fact suggest very rich state diagrams for both hard and soft particles with anisotropic interactions, featuring equilibrium phases like isotropic liquids[1–5] and nematic liquid crystals (with long-range orientational but no positional order),[1–4] as well as arrested states with slow translational and/or orientational degrees of freedom, such as orientational glasses (with slow rotations),[6–8] 'simple' glasses (with slow translations),[5] or double glasses (with slow rotations as well as translations).[5,8–10]

Several studies over the past years have demonstrated that dispersions of plate-shaped clays[4,11] and related systems[12–14] can undergo disorder-to-order transitions, and that these transitions can be true, equilibrium liquid crystal phase transitions when they occur in the ergodic sol region of the state diagrams. For Laponite (LRD) dispersions, observations of such clear-cut equilibrium transitions are generally pre-empted by dynamical

arrest. The fact that orientational order may still develop despite slow dynamics and significant viscoelasticity is nevertheless an experimentally well-established fact,[11,14–17] although in the case of Laponite (LRD), the relationship between dynamical arrest and observations of orientational order is not clear.

Here we use $C_w = 3.0$ wt% dispersions of Laponite (LRD) in deionized water to show that orientational order can develop in glassy dispersions of charged platelets when a concentration gradient is imposed through solvent evaporation. In deionized water, Laponite exists as less than 1 nm thick discs with diameters of approximately 25 nm. The particles carry a net negative surface charge and negligible rim charges. At a concentration of $C_w = 3.0$ wt% in deionized water, Laponite is reported to form orientationally disordered, repulsive 'Wigner' glasses whose translational as well as rotational dynamics slow down with time.[10,18–24] A recent study[23] indicates that interparticle attraction may gain influence at aging times beyond the timescale associated with the initial glass formation, although without altering the observed structure of the glass.

2 Experimental

We prepared our samples at $C_w = 3.0$ wt% Laponite (LRD) in deionized water following the procedure proposed by Bonn *et al.*[19] All samples were stirred for 30 min after mixing before being suction filtered through a 0.8 μm pore filter. The time of filtration is $t_w = 0$. For $t_w > 0$ the concentration of particles was either increased by slow evaporation of the solvent water, or kept constant for a set of sealed reference samples. The evaporation process was conducted either under ambient conditions or in a protected N_2 atmosphere; the procedures were found to

aDepartment of Physics, Norwegian University of Science and Technology, NO-7491 Trondheim, Norway. E-mail: lindbohansen@gmail.com

bLaboratoire Interdisciplinaire de Physique, UMR 5588, F-38041 Grenoble, France

cInstitute for Energy Technology, NO-2007 Kjeller, Norway

dMAX IV Laboratory, Lund University, SE-221 00 Lund, Sweden

eVan der Waals-Zeeman Institute, University of Amsterdam, NL-1098 XH Amsterdam, Netherlands

yield the same birefringence patterns. At waiting times in the range 2 weeks < t_w < 3 weeks, the dispersions were investigated by dynamical light scattering (non-evaporated samples), and by small-angle X-ray scattering and birefringence imaging (evaporated and non-evaporated samples). The waiting times are well beyond the timescales associated with repulsive glass formation,[22,23] and also beyond the timescale for which attractive interactions have been suggested.[23]

3 Results and discussion

Dynamical light scattering

We use dynamical light scattering (DLS, Fig. 1a) to confirm that, in agreement with previous studies,[18,22,23] our $C_w = 3.0$ wt% samples can be interpreted as glasses. Because samples are non-ergodic on the experimental timescale, the intermediate scattering function $f_v(\vec{q}, \tau)$ is obtained from the measured time autocorrelation function $g_v(\vec{q}, \tau)$ as[25–27]

$$f_v(\vec{q}, \tau) = 1 + Y((g_v(\vec{q}, \tau) - g_v(\vec{q}, 0) + 1)^{1/2} - 1). \tag{1}$$

Here $Y = \langle I(\vec{q}, \tau)\rangle_t / \langle I(\vec{q}, \tau)\rangle_e$, with $\langle I(\vec{q}, \tau)\rangle_t$ being the time-averaged brightness of the speckle yielding $g_v(\vec{q}, \tau)$, and $\langle I(\vec{q}, \tau)\rangle_e$

Fig. 1 a) DLS on $C_w = 3.0$ wt% LRD in deionized water at $t_w = 3$ weeks. The intermediate scattering functions $f_v(\vec{q}, \tau)$ and $f_h(\vec{q}, \tau)$ are obtained from the measured polarized and depolarized time autocorrelation functions, respectively. (b) SAXS data on $C_w = 2.0$ wt% and 3.0 wt% LRD in deionized water, and the scattering from an evaporated sample along the $c \parallel z$ direction (see Fig. 3c). The calc. poly curve is the form factor for a polydisperse distribution $P(h, r) \propto 1/V(h, r)$ of discs with diameters from $2r_1 = 15$ nm to $2r_2 = 35$ nm, and the $I(q) \propto q^{-2}$ curve the expected power law behaviour for discs at intermediate q. Experimental data for non-evaporated samples and calculated data largely overlap for $q \gtrsim 0.15$ nm^{-1}.

the average brightness of a large number of sampling points. The fit of $f_v(\vec{q}, \tau)$ to a function

$$f_v(\vec{q}, \tau) = A \exp(-\tau/\tau_1) + (A - 1)\exp(-(\tau/\tau_2)^\beta) \tag{2}$$

(Fig. 1a), yields $\tau_1 = 0.01$ ms and $\langle\tau_2\rangle = (\tau_2/\beta) \Gamma (1/\beta) = 7 \times 10^8$ s (with $\beta = 0.3$). Because of the limited range in τ, the latter value is a lower bound on $\langle\tau_2\rangle$. The non-ergodicity parameter, obtained from $f_v(\vec{q}, \tau)$ in the limit $\tau \rightarrow \infty$ (where $g_v(\vec{q}, \infty) = 1$), assumes values $f_v(\vec{q}, \infty) > 0.9$ at $t_w = 3$ weeks. This shows that the majority of the scattered intensity comes from density fluctuations that are frozen-in on the experimental timescale. We also attempt to assess the rotational dynamics with depolarized DLS (Fig. 1a), and measure the time autocorrelation function $g_h(\vec{q}, \tau)$ that contains contributions both from translational and rotational correlations. The nearly flat behaviour of the resulting intermediate scattering function $f_h(\vec{q}, \tau)$ suggests, in accordance with previous studies,[10] that rotational dynamics are also arrested.

Small-angle X-ray scattering from non-evaporated samples

Small-angle X-ray scattering (SAXS) experiments on such non-evaporated samples give isotropic scattering patterns indicating no net orientational order and only short-range positional order (Fig. 1b), expected from crowding (with a $C_w = 2.0$ wt% sample having less structure factor scattering than a $C_w = 3.0$ wt% one). To rationalize this, we calculate the theoretical volume V_s available to each Laponite platelet at complete delamination, assuming that N particles of a $C_w = 3.0$ wt% dispersion occupy and freely rotate within N non-overlapping spheres of radius r_s. The empirical formula for Laponite is $Na_{0.7}Mg_{5.5}Li_{0.3}Si_8O_{24}H_4$ per unit cell.[24] With each 25 nm Laponite platelet containing about $50 \times 50 = 2.5 \times 10^3$ unit cells,[28] we find that a single Laponite platelet has a molecular weight of 1.9×10^6 g mol^{-1}, so that a $C_w = 3.0$ wt% dispersion has a platelet concentration of $N/V = 9.5 \times 10^{21}$ m^{-3}, which is then also the concentration of spheres. Now, if these spheres are randomly close packed (at a packing fraction 64%), we find that a total dispersion volume V has a volume of $0.64V$ that is divided into N spheres, so that the volume per sphere is $V_s = 0.64V/N = 6.8 \times 10^{-23}$ m^3. The spheres therefore have a radius of $r_s = (3V_s/4\pi)^{1/3} = 25$ nm. Such a Laponite glass would be non-connected and structurally homogeneous on length scales above roughly 50 nm, corresponding to a structure factor $S(\vec{q}) < 1$ for $\vec{q} \lesssim 0.13$ nm^{-1}. This is in good agreement with the experimental data, which deviate from the calculated form factor for $\vec{q} \lesssim 0.15$ nm^{-1} (Fig. 1b). The DLS and SAXS data are therefore consistent with the interpretation of non-evaporated $C_w = 3.0$ wt% samples as non-connected, double glasses, with neither long-range orientational nor translational order (see Fig. 2a). For reference, we note that the above calculations based on a close packing of spheres of radius $r_s = (25/2)$ nm (with a packing fraction 74%) imply that some local ordering is geometrically required for Laponite suspensions at platelet concentrations $C_w > 29$ wt%.

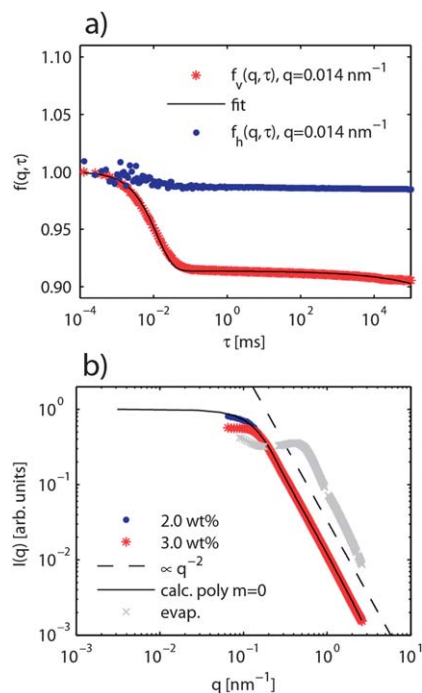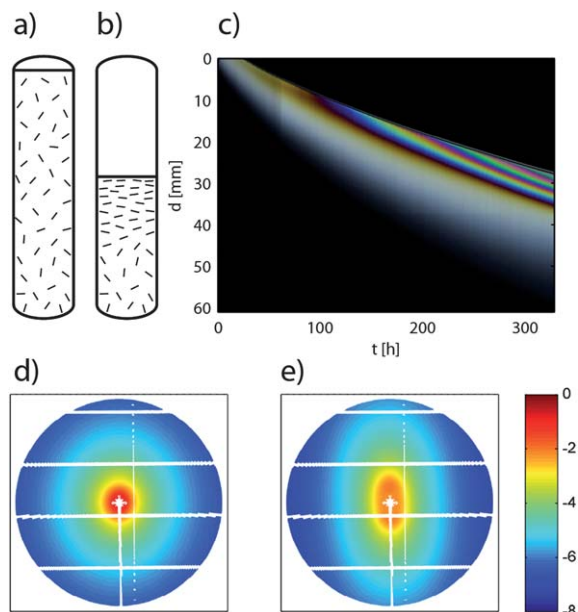**Fig. 2** a) Schematic of the structure of an isotropic Laponite glass and (b) of a Laponite glass with evaporation-induced orientational order. (c) A spatio-temporal plot of developing birefringence in an evaporating $C_w = 3.0$ wt% LRD sample, showing the central part of a capillary imaged at successive waiting times. Crossed linear polarizers were oriented at 45 deg with the vertical capillary axis. The thickness of the sample was $l = 2.65$ nm, so that 4th order magenta, appearing at the interface near the end of this time series, implies a $\Delta n = 8.3 \times 10^{-4}$. (d) SAXS pattern collected from the sample imaged in (c) at a distance of 10 mm from the interface, at the end of the time series, and (e) just below the interface.

Small-angle X-ray scattering and birefringence from evaporated samples

Whereas SAXS data from non-evaporated samples are isotropic, the data collected on samples from which evaporation has occurred are anisotropic (see Fig. 2d and e). A spatio-temporal plot of the evaporation process (Fig. 2c) shows birefringence that grows from the evaporation interface towards the bulk, invading the sample on macroscopic length scales on the order of cm in a matter of weeks. Because the birefringence remains unchanged when samples are rotated by an angle θ around their cylinder axis $c \parallel z$, the ordering must necessarily constitute a cylindrically symmetric distribution of particle normals $\vec{n}$ around this direction. The successive changes of the birefringence colours (determined by the retardation $\Delta n l$, with l being the sample thickness) signal the existence of a long-lived gradient in either the order (as characterized e.g. via the nematic order parameter S_2), in the concentration of particles (or equivalently the volume fraction Φ), or both (because $\Delta n \propto S_2 \Phi$).[17]

We confirm the presence of a gradient in Φ with X-ray transmission, following previous work by Fonseca et al.[29] From this analysis, volume fractions around $\Phi = 2\%$ are obtained in non-evaporated samples or in evaporated ones far away from the interface, whereas close to the interface the volume fraction gradually rises, reaching above $\Phi = 6\%$ in some cases. By converting volume fraction data to particle concentrations, we find that the concentration near the interface exceeds $C_w = 9$ wt%,

reaching well into the range in which Mourchid et al.[16] have observed textures reminiscent of nematic defects in Laponite (LRD) dispersions, but where simulations yield arrested dynamics without order.[30] A significant structure factor contribution to the scattering signal accompanies the concentration gradient, with correlation peaks becoming progressively more pronounced as the concentration increases. Near the interface, the maximum deviation from the calculated form factor occurs around $q = 0.57$ nm^{-1} (Fig. 1b), roughly corresponding to characteristic distances in real space of $2\pi/q = 11$ nm. The peaks share the anisotropy of the overall scattering patterns (see Fig. 2e), and therefore likely represent a typical face-to-face distance between approximately parallel platelets; for a given center–center separation, this configuration minimizes the repulsion between discs interacting via a purely repulsive potential,[31,32] and minimizes the excluded volume.

Calculating the order parameter

To assess whether a gradient in the order parameter S_2 exists in evaporated samples, we compare the anisotropy in the measured SAXS data to simulated SAXS patterns computed with a suitable orientational distribution.[17,33,34] In our computations we use a structure factor $S(\vec{q}) = 1$ and Fournet's expression[35] for the form factor of a cylindrical disc of height h and radius r to approximate the form factor of a Laponite particle through

$$F(q, \gamma, h, r) = K \frac{\sin((qh\cos\gamma)/2)}{(qh\cos\gamma)/2} \frac{2J_1(qr\sin\gamma)}{qr\sin\gamma}. \quad (3)$$

Here γ is the angle between the scattering vector $\vec{q}$ and the disc normal $\vec{n}$ (see Fig. 3a) and J_1 the first order Bessel function of the first kind. For the orientational distribution of disc normals we use the classical Maier–Saupe distribution[36–38]

$$f(\theta, m) = C(m)\exp(m\cos^2\theta). \quad (4)$$

The function is normalized to one over half the unit sphere because opposite orientations of $\vec{n}$ correspond to identical physical orientations of a platelet. The parameter $m \geq 0$ determines the narrowness of the distribution of $\vec{n}$ around z and yields S_2 as

$$S_2(m) = 2\pi \int_0^{\pi/2} \left(\frac{3\cos^2\theta - 1}{2}\right) f(\theta, m)\sin\theta\,d\theta. \quad (5)$$

We express the angle γ between $\vec{q}$ and $\vec{n}$ via θ and ϕ (which fixes the orientation of $\vec{n}$ in the lab frame) and α (which fixes the direction of $\vec{q}$ in the x, z-plane) so that trigonometry gives

$$\gamma(\theta, \phi, \alpha) = \cos^{-1}(\sin\theta\cos\phi\cos\alpha + \cos\theta\sin\alpha). \quad (6)$$

The q- and α-dependent intensity on the detector for a given order as specified by m is then found by numerical integration of the squared form factor weighted by the orientational distribution. The integral is written as

$$I(q, \alpha, h, r, m) = K^2 \int_{r_1}^{r_2} \int_0^{2\pi} \int_0^{\pi/2} \xi f(\theta, m)\sin\theta\,d\theta\,d\phi\,dr, \quad (7)$$
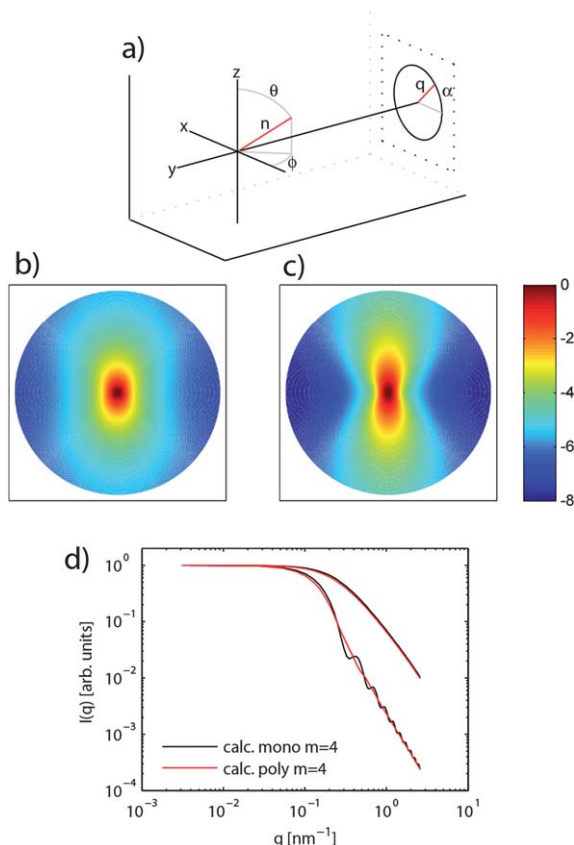
Fig. 3 a) Scattering geometry with the X-ray beam incident along the y-axis, the capillary axis c ∥ z, and the detector plane parallel to the x, z-plane. (b) Simulated SAXS pattern with $m = 1.46$ and $S_2 = 0.21$ for a polydisperse distribution of discs with diameters in the range from $2r_1 = 15$ nm to $2r_2 = 35$ nm. The intensity scale is logarithmic, and the q-range 0.003 nm$^{-1} \leq q \leq 2.6$ nm^{-1}. (c) Simulated SAXS pattern for a polydisperse distribution with $m = 4.00$ and $S_2 = 0.55$. (d) One-dimensional plots of the calculated scattered intensity from (c) along respectively the horizontal and vertical directions, along with the intensity calculated for an equally ordered monodisperse distribution of discs with diameter $2r = 25$ nm.

with

$$\xi = P(h, r)[V(h, r)F(q, \gamma (\theta, \phi, \alpha), h, r)]^2. \tag{8}$$

Here we have used the locally monodisperse approximation[39] and integrated also over a distribution $P(h, r) \propto 1/V(h, r)$ of radii r, with $V(h, r)$ being the volume of a disc. We use a polydisperse distribution spanning the range from $2r_1 = 15$ nm to $2r_2 = 35$ nm; this empirical choice fits the isotropic data (Fig. 1b) and allows for a smoothly decaying intensity also when the degree of order is higher. The resulting two-dimensional scattering patterns (Fig. 3b and c) become progressively more anisotropic as m is increased, with the isointensity lines at small q being roughly elliptical whereas the isointensity lines at higher q show a 'butterfly' pattern. The effect of including size-polydispersity when $P(h, r) \propto 1/V(h, r)$ (see Fig. 3d) is effectively to smear out the oscillations which are prominent for a monodisperse system.

Orientational order *versus* volume fraction

We compare the calculated SAXS patterns for different S_2 with the experimental data in the q-range where the structure factor

is flat ($S(\vec{q}) = 1$). The fitting procedure (after the parameters r_1, r_2 and h were determined from the isotropic data) involves finding the m-parameter which produces a calculated pattern whose anisotropy most closely matches the experimentally measured anisotropy. From this analysis, we find that even our most anisotropic SAXS patterns measured correspond to relatively low values of the order parameter, $S_2 \lesssim 0.21$. This is in contrast to what was found by Lemaire *et al.*[17] for similarly sized Laponite B dispersions, where uniform order around $S_2 = 0.55$ was reported. We also find that the relationship between S_2 and Φ (Fig. 4a) appears relatively well-defined within the uncertainty associated with our measurements, and that this relationship reproduces across the investigated samples. The observed order grows continuously from around zero and qualitatively follows Φ in a manner reminiscent of the expected dependence of S_2 on Φ for isotropic–nematic transitions in an ordering field,[40–42] for which the free energy F may be expanded in powers of the order parameter so that

$$F = F_0 + \sigma S_2 + c_2 S_2{}^2 + c_3 S_2{}^3 + c_4 S_2{}^4. \tag{9}$$

Here F_0 is the reference energy for the isotropic system and σ the strength of the ordering field; c_3 and c_4 are parameters that change sufficiently slowly in the vicinity of the phase transition so that the prefactor $c_2 = b (\Phi^* - \Phi)^2$ is the only parameter which depends on Φ. By setting the partial derivative of the expansion to zero, the equilibrium value for S_2 follows from

$$\frac{\partial F}{\partial S_2} = \sigma + 2c_2 S_2 + 3c_3 S_2{}^2 + 4c_4 S_2{}^3 = 0. \tag{10}$$

We find that, assuming an underlying very weakly first order transition, we can fit our measurements for S_2 and Φ with such a dependence (Fig. 4a). We however stress that the free energy minimization approach only applies if a shift in order away from the observed S_2 at any given Φ drives the system upwards in the free energy landscape.
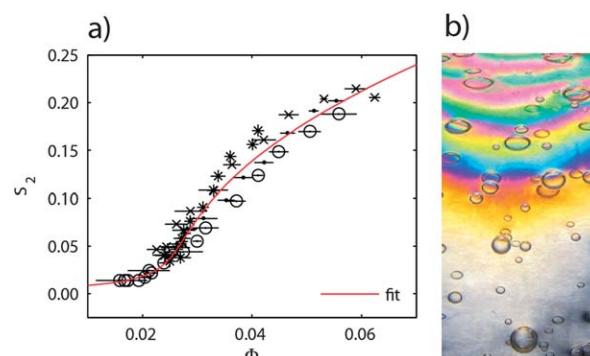

Fig. 4 a) Estimated order parameter S_2 *versus* the volume fraction of LRD particles Φ. The error bars represent the standard deviation on the mean of the volume fraction from several transmission measurements, and the different symbols represent data from a set of equivalently treated samples. The solid line shows the best fit of a function inspired by an extended Landau–de Gennes model to the data, as described in the text. (b) Birefringence image of a Laponite sample with air bubbles.

History dependent order

The origin of orientational order in Laponite (LRD) dispersions has been an unresolved issue in the literature.[24] Mourchid et al.[16] early on observed textures reminiscent of nematic defects in samples with significant viscoelasticity. A later study of oedometrically compressed samples with NMR[43] found orientational order developing with the concentration in a manner similar to that found in our samples (Fig. 4a), albeit at higher salt concentrations. The compression study predicts perfect order at very high volume fractions; this is similar to what is predicted by the empirical fit to our data (Fig. 4a), where an order parameter of $S_2 = 1.0$ is achieved when $\Phi = 90\%$.

Well before such high volume fractions are reached however, we note that samples are prone to fracture, pointing to the evaporation process causing significant stresses on the glass. We also observe that implanted air bubbles which are spherical in the bulk (or near the interface prior to evaporation) become progressively more oblate towards the evaporating interface, with the unique, short axis of oblate bubbles pointing along the capillary axis $c \parallel z$ (see Fig. 4b). From the spatio-temporal birefringence data (Fig. 2c), we estimate that evaporation-induced compression of the colloidal structure causes an average normal rate of deformation of 4×10^{-7} s^{-1}; this value is two orders of magnitude larger than the inverse of the estimated structural relaxation time $1/\langle\tau_2\rangle = 1 \times 10^{-9}$ s^{-1} from DLS (Fig. 1a). This implies that the response of $C_w = 3.0$ wt% Laponite (LRD) dispersions to such strain rates is solid-like, i.e. is elastic or plastic. Plastic events, which involve irreversible displacements or reorientations in response to stress, are known to impart permanent anisotropies to e.g. simulated, sheared silica glasses.[44] However, although such plastic events drive the system from less to more favoured configurations under stress, it is important to note that the order resulting from deformations is generally not intrinsic but history-dependent. Monte-Carlo simulations[32] of highly charged platelets of the same size as Laponite (at ionic strengths comparable to our study[21]) suggest that the density at the orientational order–disorder transition corresponds to $\Phi = 12\%$.[32] This volume fraction is considerably higher than the range of volume fractions we explore, supporting the hypothesis that the weak orientational ordering seen in our experiments has a different origin than that which would arise spontaneously from excluded volume effects and electrostatic interactions.

4 Conclusions

Based on our observations, we conclude that the orientational order observed in our Laponite (LRD) samples results from plastic deformation of the colloidal glass in response to compression caused by evaporation. That the order nevertheless should follow the volume fraction is not unexpected since the evolution of both parameters within this picture follows the compression. One might imagine a situation where, despite the quite obviously slow translational dynamics, the rotational degrees of freedom associated with $\vec{n}$ were able to equilibrate. The slow decay of depolarized correlations in the DLS data

argues against this possibility. We therefore conclude that the birefringence in our samples is due to plastic deformations driving the initially disordered glass into a state where a long-lived concentration gradient is accompanied by orientational order and increasingly pronounced interparticle correlations.

References

1 L. Onsager, *Ann. N. Y. Acad. Sci.*, 1949, **51**, 627–659.
2 R. Eppenga and D. Frenkel, *Mol. Phys.*, 1984, **52**, 1303–1334.
3 D. Frenkel and B. M. Mulder, *Mol. Phys.*, 1985, **55**, 1171–1192.
4 L. J. Michot, I. Bihannic, S. Maddi, S. S. Funari, C. Baravian, P. Levitz and P. Davidson, *Proc. Natl. Acad. Sci. U. S. A.*, 2006, **103**, 16101–16104.
5 R. Zhang and K. S. Schweizer, *Phys. Rev. E: Stat., Nonlinear, Soft Matter Phys.*, 2009, **80**, 011502.
6 M. Letz, R. Schilling and A. Latz, *Phys. Rev. E: Stat. Phys., Plasmas, Fluids, Relat. Interdisc. Top.*, 2000, **62**, 5173–5178.
7 C. De Michele, R. Schilling and F. Sciortino, *Phys. Rev. Lett.*, 2007, **98**, 265702.
8 Z. Zheng, F. Wang and Y. Han, *Phys. Rev. Lett.*, 2011, **107**, 065702.
9 P. Pfleiderer, K. Milinkovic and T. Schilling, *Europhys. Lett.*, 2008, **84**, 16003.
10 S. Jabbari-Farouji, G. H. Wegdam and D. Bonn, *Phys. Rev. E: Stat., Nonlinear, Soft Matter Phys.*, 2012, **86**, 041401.
11 J. O. Fossum, E. Gudding, D. D. M. Fonseca, Y. Meheust, E. DiMasi, T. Gog and C. Venkataraman, *Energy*, 2005, **30**, 873–883.
12 D. van der Beek and H. N. W. Lekkerkerker, *Langmuir*, 2004, **20**, 8582–8586.
13 J. Zhang, L. Y. Luan, W. X. Zhu, S. Y. Liu and D. J. Sun, *Langmuir*, 2007, **23**, 5331–5337.
14 M. C. D. Mourad, D. V. Byelov, A. V. Petukhov and H. N. W. Lekkerkerker, *J. Phys.: Condens. Matter*, 2008, **20**, 494201.
15 J. C. P. Gabriel, C. Sanchez and P. Davidson, *J. Phys. Chem.*, 1996, **100**, 11139–11143.
16 A. Mourchid, E. Lecolier, H. Van Damme and P. Levitz, *Langmuir*, 1998, **14**, 4718–4723.
17 B. J. Lemaire, P. Panine, J. C. P. Gabriel and P. Davidson, *Europhys. Lett.*, 2002, **59**, 55–61.
18 D. Bonn, J. Tanaka, G. Wegdam, H. Kellay and J. Meunier, *Europhys. Lett.*, 1999, **45**, 52–57.
19 D. Bonn, H. Kellay, H. Tanaka, G. Wegdam and J. Meunier, *Langmuir*, 1999, **15**, 7534–7536.
20 H. Tanaka, J. Meunier and D. Bonn, *Phys. Rev. E: Stat., Nonlinear, Soft Matter Phys.*, 2004, **69**, 031404.
21 H. Tanaka, S. Jabbari-Farouji, J. Meunier and D. Bonn, *Phys. Rev. E: Stat., Nonlinear, Soft Matter Phys.*, 2005, **71**, 021402.

22 S. Jabbari-Farouji, G. H. Wegdam and D. Bonn, *Phys. Rev. Lett.*, 2007, **99**, 065701.

23 B. Ruzicka, L. Zulian, E. Zaccarelli, R. Angelini, M. Sztucki, A. Moussaid and G. Ruocco, *Phys. Rev. Lett.*, 2010, **104**, 085701.

24 B. Ruzicka and E. Zaccarelli, *Soft Matter*, 2011, **7**, 1268–1286.

25 P. N. Pusey and W. Vanmegen, *Phys. A*, 1989, **157**, 705–741.

26 W. Vanmegen, S. M. Underwood and P. N. Pusey, *Phys. Rev. Lett.*, 1991, **67**, 1586–1589.

27 M. Kroon, G. H. Wegdam and R. Sprik, *Phys. Rev. E: Stat. Phys., Plasmas, Fluids, Relat. Interdiscip. Top.*, 1996, **54**, 6541–6550.

28 Y. Aray, M. Marquez, J. Rodriguez, S. Coll, Y. Simon-Manso, C. Gonzalez and D. A. Weitz, *J. Phys. Chem. B*, 2003, **107**, 8946–8952.

29 D. M. Fonseca, Y. Meheust, J. O. Fossum, K. D. Knudsen and K. P. S. Parmar, *Phys. Rev. E: Stat., Nonlinear, Soft Matter Phys.*, 2009, **79**, 021402.

30 S. Mossa, C. De Michele and F. Sciortino, *J. Chem. Phys.*, 2007, **126**, 014905.

31 R. Agra, E. Trizac and L. Bocquet, *Eur. Phys. J. E*, 2004, **15**, 345–357.

32 S. Jabbari-Farouji, J.-J. Weis, P. Davidson, P. Levitz and E. Trizac, arXiv:1212.5043 [cond-mat.soft], 2012.

33 Y. Méheust, S. Dagois-Bohy, K. D. Knudsen and J. O. Fossum, *J. Appl. Crystallogr.*, 2007, **40**, s286–s291.

34 I. Bihannic, C. Baravian, J. F. L. Duval, E. Paineau, F. Meneau, P. Levitz, J. P. de Silva, P. Davidson and L. J. Michot, *J. Phys. Chem. B*, 2010, **114**, 16347–16355.

35 G. Fournet, *Bull. Soc. Fr. Mineral. Cristallogr.*, 1951, **74**, 37–172.

36 W. Maier and A. Saupe, *Z. Naturforsch., A: Astrophys., Phys. Phys. Chem.*, 1958, **13**, 564–566.

37 W. Maier and A. Saupe, *Z. Naturforsch., A: Astrophys., Phys. Phys. Chem.*, 1959, **14**, 882–889.

38 W. Maier and A. Saupe, *Z. Naturforsch., A: Astrophys., Phys. Phys. Chem.*, 1960, **15**, 287–292.

39 J. S. Pedersen, *J. Appl. Crystallogr.*, 1994, **27**, 595–608.

40 P. de Gennes, *Phys. Lett. A*, 1969, **30**, 454–455.

41 P. de Gennes, *Solid State Commun.*, 1972, **10**, 753–756.

42 E. F. Gramsbergen, L. Longa and W. H. Dejeu, *Phys. Rep.*, 1986, **135**, 195.

43 P. Porion, M. Al-Mukhtar, A. M. Faugere and A. Delville, *J. Phys. Chem. B*, 2004, **108**, 10825–10831.

44 C. L. Rountree, D. Vandembroucq, M. Talamali, E. Bouchaud and S. Roux, *Phys. Rev. Lett.*, 2009, **102**, 195501.

45 A. Labrador, Y. Cerenius, C. Svensson, K. Theodor and T. Plivelic, *J. Phys. Conf. Ser.*, 2013, **425**, 072019.